ACSNANO

www.acsnano.org

ARTICLE

Injectable Hydrogels Encapsulating Dual-Functional Au@Pt Core–Shell Nanoparticles Regulate Infarcted Microenvironments and Enhance the Therapeutic Efficacy of Stem Cells through Antioxidant and Electrical Integration

Wei Liu,[⊥] Nana Zhao,[⊥] Qi Yin, Xiaoyi Zhao, Kangli Guo, Yifan Xian, Siwei Li, Chunlan Wang, Miaomiao Zhu, Yurong Du, Fu-Jian Xu,* Changyong Wang,* and Jin Zhou*

Cite This: *ACS Nano* 2023, 17, 2053–2066

Read Online

ACCESS | Metrics & More | Article Recommendations | Supporting Information

ABSTRACT: **Injectable functional biomaterials have made significant progress in cardiac regenerative. In addition, how to adjust the abominable infarction microenvironment and introduce therapeutic stem cells to improve the healing effect has become a hotspot. Herein, injectable stem cell vector is prepared by combining natural alginate hydrogel and Au@Pt nanoparticles (Au@Pt/Alg hydrogel) to encapsulate brown adipose stem cells (BASCs). Au@Pt nanoparticles with both antioxidative and conductive properties could effectively eliminate reactive oxygen species, enhance the frequency of action potential release of cardiomyocytes, and further reduce the inflammatory factors of macrophage *in vitro*. The Au@Pt/Alg hydrogel enhances the antioxidant, differentiation, and paracrine capability of BASCs. The effect of BASCs loaded Au@Pt/Alg hydrogel is evaluated in a rat myocardial infarction (MI) model. The antioxidant, anti-inflammatory, and heart electrical integration are showed in the MI model. More interestingly, Au@Pt/Alg hydrogel can effectively maintain the paracrine efficiency and pro-angiogenesis effects of BASCs in the infarcted area. This study led us to recognize the great value of Au@Pt/Alg hydrogels for their ability to actively regulate the microenvironment and carry stem cells for MI treatment.**

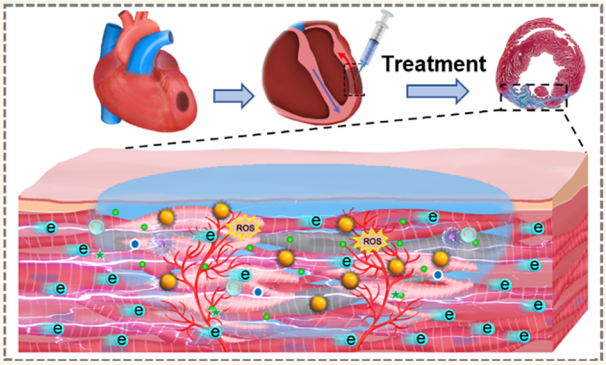

KEYWORDS: *Au@Pt nanoparticles, alginate hydrogel, stem cell, myocardial infarction, cardiac repair*

INTRODUCTION

Myocardial infarction (MI) exhibits high morbidity and mortality,[1] and a series of studies have shown that the use of biomaterials for MI treatment have made important progress.[2] In addition, biomaterials are important in constructing engineered heart tissue (ECTs) and the repair of ECTs after transplantation.[3,4] On the other hand, biomaterials as stem cell carriers could improve their therapeutic efficacy.[5,6] However, the ischemic, hypoxic, and inflammatory MI microenvironment severely limits the survival and function of ECTs or stem cells. Therefore, researchers are paying more attention to the infarcted microenvironment by introducing specific functional groups or bioactive substances into biomaterials to intelligently respond and regulate the microenvironment of the diseased tissue.[7] A series of functional injectable hydrogels promote MI repair by regulating inflammation, inhibiting myocardial apoptosis, and promoting angiogenesis.[8−10] We recently developed a natural melanin/alginate hydrogel with obvious

Received: July 26, 2022
Accepted: January 20, 2023
Published: January 25, 2023

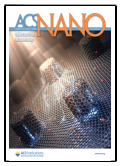

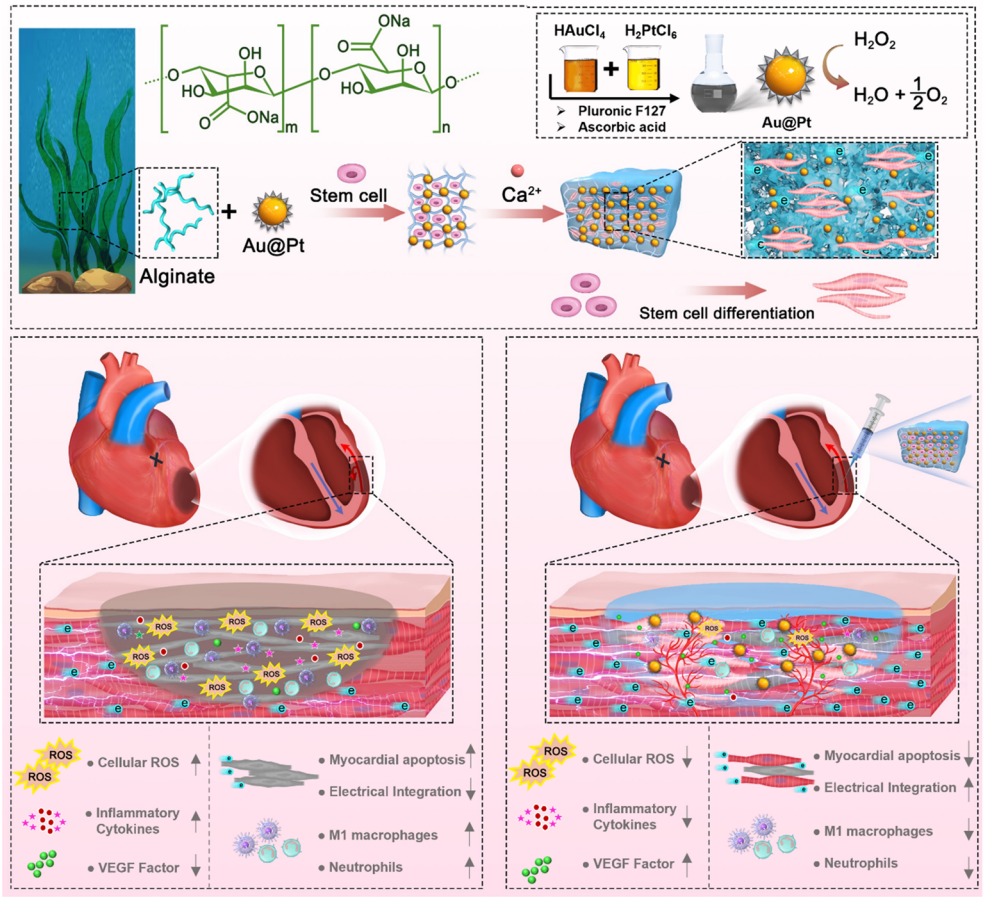

Figure 1. Schematic illustration of the preparation and therapeutic mechanism of Au@Pt/Alg hydrogel carried BASCs in cardiac repair in vivo.

antioxidant function. The hydrogel has a good ability to adjust the inflammatory and reactive oxygen species (ROS) at the early MI, realizing obvious cardiac regeneration and repair.[11] How to use biomaterials to reverse the early MI microenvironment and further endow it with the ability to promote repair is the key to improving the therapeutic effect.

In addition, how to reconstruct the conductive microenvironment of infarcted myocardium to promote electrical conduction and electrical integration is the goal of cardiac regeneration, and it is also the focus of researchers in the design of biomaterials to promote cardiac repair in recent years. At present, researchers have used conductive gold nanoparticles (AuNPs),[12] carbon-based conductive materials,[13] conductive polymers,[14] and other conductive nanomaterials to improve the conductivity and electrical pulses on scar tissue. AuNPs have been widely used in a range of biological and medical research through their controllable geometric structure and optical and surface properties, which show low cytotoxicity and biocompatibility. They are usually used in medical applications including diagnostics, sensing, molecular imaging, cancer therapy and stem cell tracking.[15−17] In addition, AuNPs are ideal nanomaterials for MI repair due to their high electrical conductivity, good biocompatibility, and facile surface modification.[18] Although AuNPs have electrical conductivity ability, the high ROS level in MI microenvironment seriously damaged cardiomyocytes and implanted stem cells. Pt nanoparticles possess catalytic and antioxidant activities. However, due to the high cost of Pt, the facile synthesis of bimetallic nanoparticles with high Pt surface area is ideal.[19] In comparison to Pt alone, core−shell Au@Pt nanoparticles (Au@Pt NPs) with a dendritic Pt shell could not only reduce the usage of Pt but also enhance the free radical scavenging ability.[20,21] Therefore, it is desirable to elucidate the untilization of Au@Pt NPs with the combination of stem cells in the MI region.

Herein, Au@Pt nanoparticles/alginate (Au@Pt/Alg) hydrogels were constructed through divalent cation (Ca^{2+}) cross-linking to regulate oxidative stress and enhance electrical conductivity. Further, stem cells were loaded with Au@Pt/Alg hydrogel, and their effects on electrical integration and cardiac function were evaluated (Figure 1). Au@Pt/Alg hydrogel can promote the survival of myocardial cells and brown adipose stem cells (BASCs) by ROS scavenging, as well as the differentiation and paracrine capability of BASCs on cardiomyocytes (CMs). In addition, Au@Pt/Alg hydrogel loaded with BASCs was injected into rat MI areas, and it was found that Au@Pt/Alg hydrogels could effectively reduce ROS level, improve retention and survival of implanted BASCs, induce angiogenesis, and promote electrical conduction velocity in MI region and effectively promote cardiac function recovery. The current research is a attempt of multifunctional microenvironment regulation biomaterials and stem cell transplantation in the treatment of MI, which would provide valuable information for the development of MI treatment strategies.

https://doi.org/10.1021/acsnano.2c07436
ACS Nano 2023, 17, 2053−2066

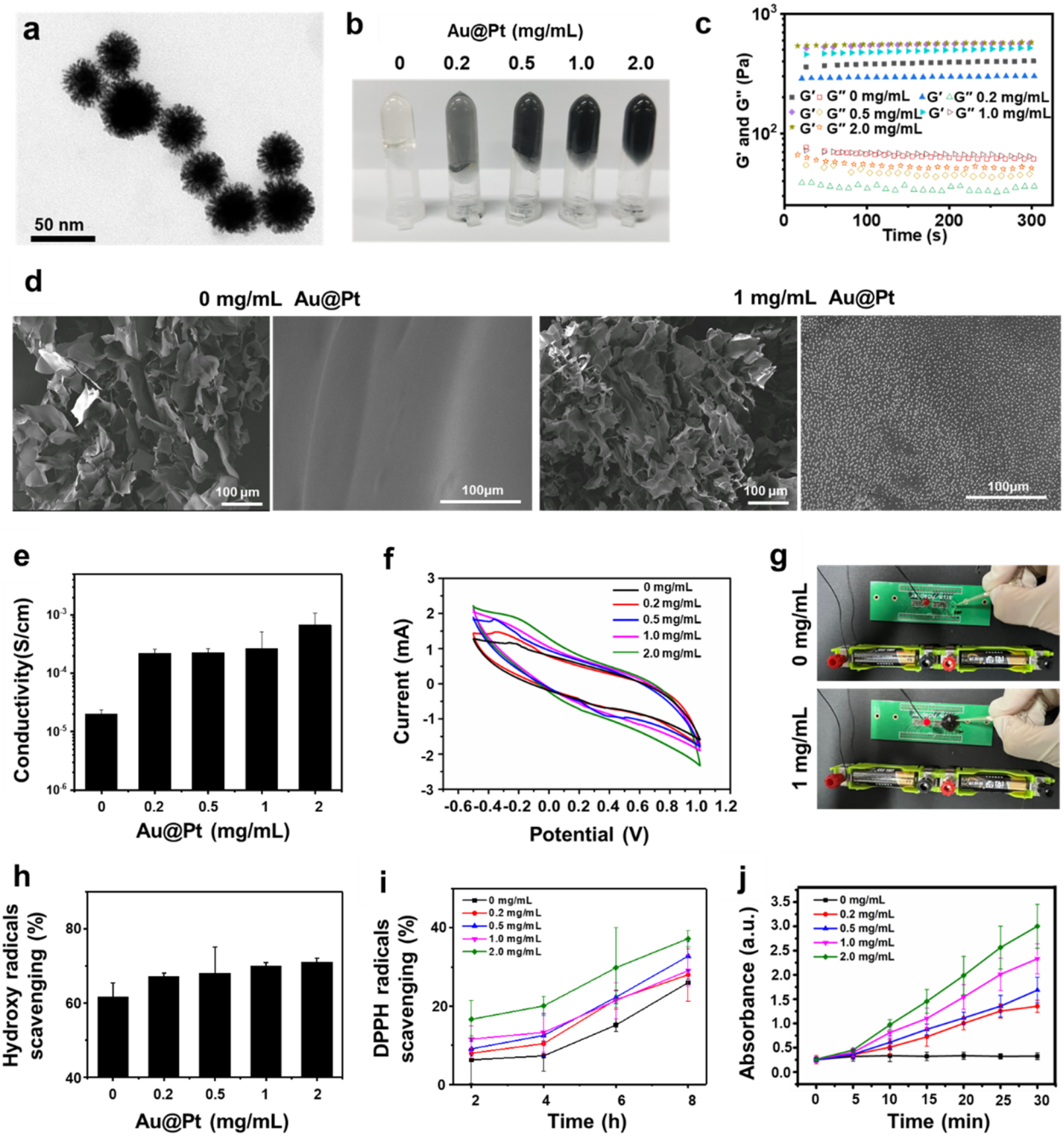

Figure 2. Preparation and characterization of Au@Pt/Alg hydrogels. (a) TEM images of Au@Pt NPs. (b) Photographs of Au@Pt/Alg hydrogels with different Au@Pt NP concentrations. (c) Rheological analysis of Au@Pt/Alg hydrogels in a time sweep mode at 37 °C. Solid symbols stand for storage modulus G' while hollow symbols stand for loss modulus G''. (d) SEM images of surfaces of Alg hydrogel and 1 mg/mLAu@Pt/Alg hydrogel. Conductivity evaluation of Au@Pt/Alg hydrogel on (e) conductivity and (f) CV curves. (g) Demonstration of a circuit with an LED showing that 1 mg/mL Au@Pt/Alg hydrogel could lighten the LED. Scavenging effect of Au@Pt/Alg hydrogels on (h) $^{\bullet}OH$, (i) DPPH radicals, and (j) H_2O_2 (mean ± SD, n = 3).

RESULTS AND DISCUSSION

Characterization of Au@Pt/Alg Hydrogel. In Figure 1, Au@Pt NPs were obtained by utilizing a surfactant-assisted process with an ultrasonic irradiation treatment.[22] As shown in the transmission electron microscopy (TEM) image (Figure 2a), Au@Pt NPs demonstrate a dendritic morphology and the diameter was ~50 ± 20 nm (Figure S1). Pt nanoparticles were homogeneous distributed on the surface of AuNPs. Then the obtained nanoparticles were added to sodium alginate and the cross-linking of sodium alginate chains was induced with calcium gluconate. As a result, homogeneous Au@Pt/Alg hydrogels were obtained within 10 min. Au@Pt was well dispersed in Au@Pt/Alg hydrogels, with the increasing of Au@Pt NPs concentration, the color of the hydrogel gradually darkened. (Figure 2b). The gelation kinetics Au@Pt/Alg hydrogels was analyzed (Figure 2c and Figure S2). It showed that the storage modulus (G') of Au@Pt/Alg hydrogels was higher than the loss modulus (G'') in different concentration Au@Pt/Alg hydrogels groupL. G' values range from 380 to 600 Pa, providing the mechanical strength is contribute to MI

https://doi.org/10.1021/acsnano.2c07436
ACS Nano 2023, 17, 2053−2066

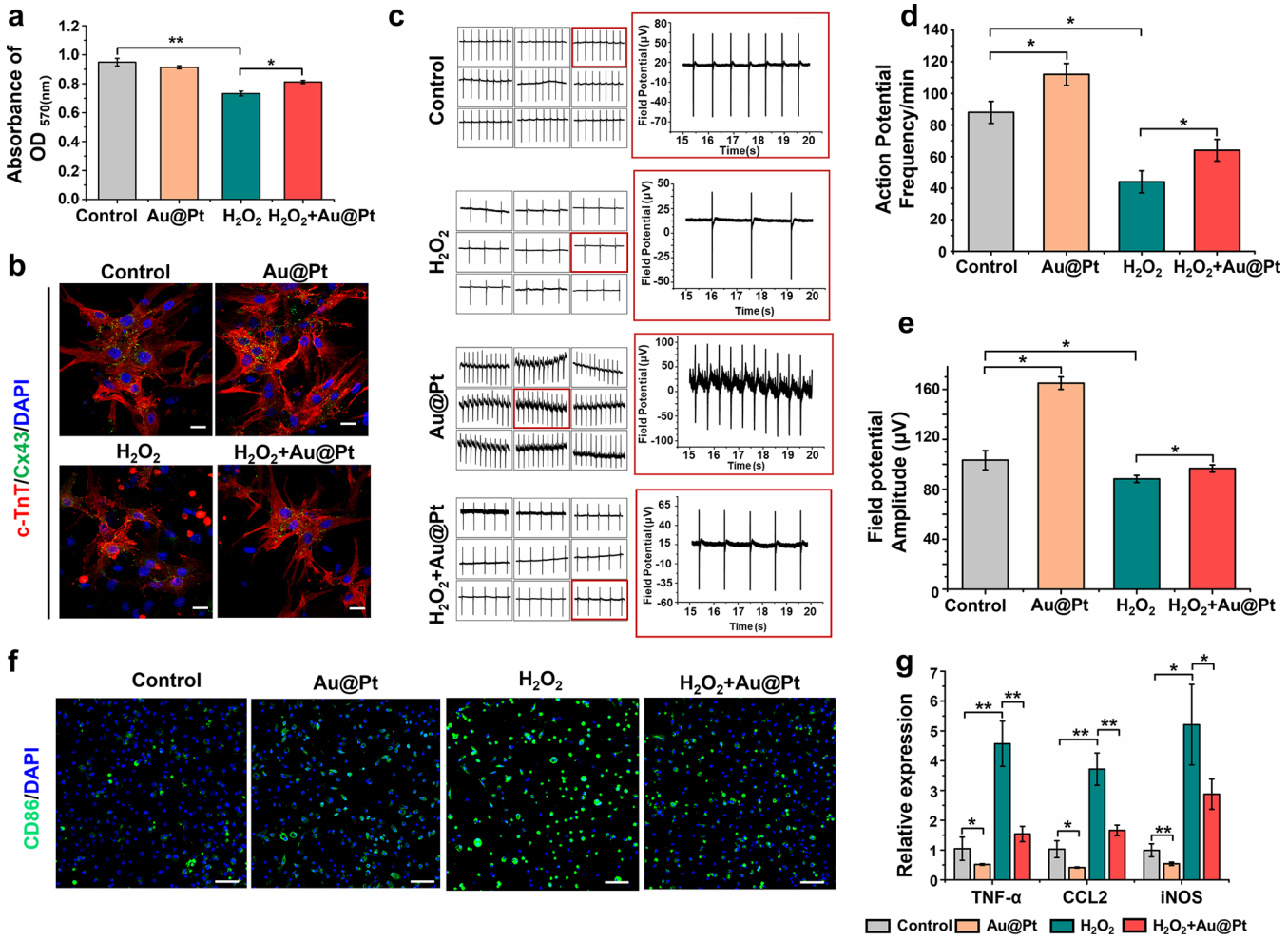

Figure 3. Effect of Au@Pt on the CMs and macrophage in ROS microenvironment. (a) Viability of CMs incubated with different treatments for 3 days. (b) Expression of c-TnT and Cx43 in CMs by immunostaining. Scale bar: 50 μm. (c) Representative electrograms of CMs with different treatmentsfor 3 days on MEA. (d) Action potential firing frequency and (e) field potential amplitude based on electrograms. (f) Representative immunofluorescence images of CD86 with different treatments in BMDMs for 1 day. Scale bar: 100 μm. (g) Inflammatory genes (TNF-α, CCL-2, iNOS) in BMDMs with different treatments detected by qRT-PCR (Au@Pt:1 mg/mL, H_2O_2: 200 μM, mean ± SD, n = 3, *p < 0.05 and **p < 0.01, Student's t test).

repair. As displayed in Figure S2a, the Au@Pt/Alg hydrogels can be conveniently injected through a syringe without clogging and remain in a stable state. The shear-thinning capability of the hydrogel was demonstrated by the results of shear-dependent-viscosity testing, confirming the injectability of the hydrogels (Figure S2b). The yield stress was calculated to be ~43.0 Pa by fitting the Herschel−Bulkley model to the flow curve (Figure S2c).

In general, cardiac patches showed higher mechanical strength when used for MI repair, it is often subject to mechanical stress.[23] However, mechanical strength of injectable hydrogels is not the critical factor for MI repair. The hydrogel may be more conducive to the transmission of mechanical signals, resulting in more coordinated cardiac tissue pulsation. Both Alg hydrogels and Au@Pt/Alg hydrogels showed a uniform porous structure in Figure 2d. The Alg hydrogel showed a flat surface morphology and Au@Pt NPs can be observed on Au@Pt/Alg hydrogels. The rough surface of Au@Pt/Alg hydrogel is conducive to the adhesion of cells in MI area and further facilitates the repair of MI. In order to prove whether Au@Pt NPs can effectively improve the electrical conductivity of Alg hydrogels, the resistivity of different concentrations of Au@Pt/Alg hydrogels (0.2, 0.5, 1, and 2 mg/mL) was measured (Figure 2e). The results showed that when 0.2 mg/mL Au@Pt was added, the conductivity of Au@Pt/Alg hydrogel increased by an order of magnitude compared with Alg hydrogel, and the conductivity of Au@Pt/Alg hydrogel did not increase significantly when Au@Pt NPs concentration increased. The conductivity of Au@Pt/Alg hydrogel was stable in Au@Pt NPs concentration range of 0.2−2 mg/mL. Moreover, the conductivity of Au@Pt/Alg hydrogel is similar to that of the natural myocardium, suggesting that it has apparent advantages in promoting regional electrical conduction of MI. In addition, Pt nanoparticles with comparable size and morphology were synthesized (Figure S3), and the electrical conductivity of Pt/Alg hydrogel was studied. It was found that the electrical conductivity of Au@Pt/Alg hydrogel (2.66×10^{-4} S/cm) was higher than that of Pt/Alg hydrogel (6.36×10^{-5} S/cm) when the nanoparticle concentration was 1 mg/mL, indicating the superiority of Au@Pt NPs. Consistent with reference reports, synthesis of bimetallic nanoparticles with high Pt surface area is ideal due to the high cost of platinum. Core−shell Au@Pt NPs with dendritic Pt shells can not only reduce the use of Pt but

https://doi.org/10.1021/acsnano.2c07436
ACS Nano 2023, 17, 2053−2066

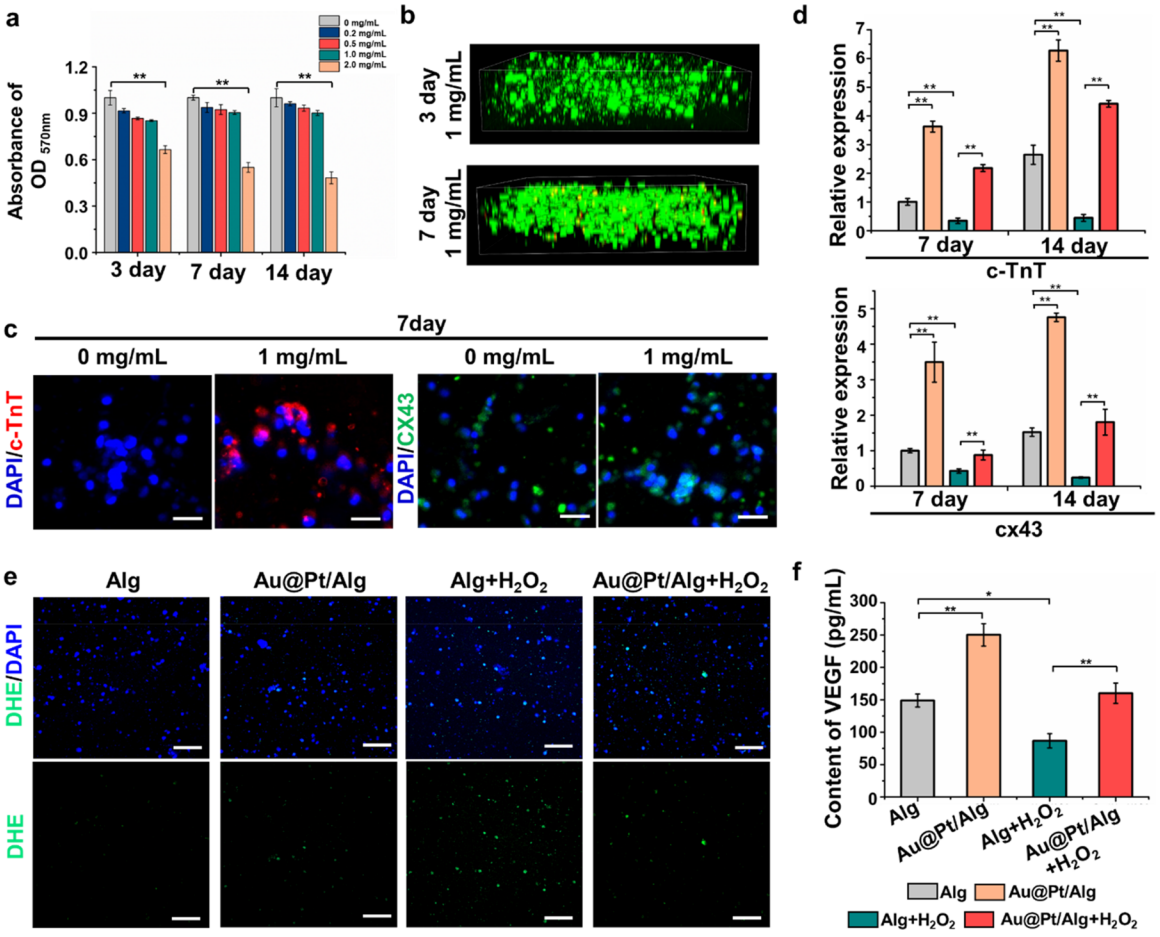

Figure 4. Effect of Au@Pt/Alg hydrogels on the BASCs. (a) Viability of BASCs seeded in Au@Pt/Alg hydrogel with different concertations for 3 days, 7 days, and 14days. (b) Distribution of live and dead BASCs cells in 1 mg/mLAu@Pt/Alg hydrogel by live/dead staining on day 3 and day 7. (c) Expression of c-TnT, Cx43 in BASCs by immunostaining and (d) qRT-PCR. Scale bar: 100 μm. (e) Representative fluorescent images of intracellular superoxide anion radical activity (DHE) of BASCs in 1 mg/mL Au@Pt/Alg hydrogel on day 1. Scale bar: 100 μm. (f) VEGF paracrine of BASCs in 1 mg/mL Au@Pt/Alg hydrogel on day 7 (mean ± SD, n = 3, *p < 0.05 and **p < 0.01, Student's t test).

also enhance its good conductive properties compared to Pt alone. At the same time, electrochemical properties of Au@Pt/Alg hydrogels were indirectly characterized by detecting voltammetry cycle (CV) curve. The curve area formed by hydrogel became larger and the curve rise became steeper with the increase of Au@Pt concentration (Figure 2f). The result indicates an increase in charge storage capacity and electrical activity. Adding Au@Pt NPs makes the hydrogel have low interfacial charge transfer impedance and a fast electron transfer rate. Further, simple Alg hydrogel and 1 mg/mL Au@Pt/Alg hydrogel were selected for an LED circuit experiment (Figure 2g) to verify the transmission of electrical signals. The results showed that the addition of 1 mg/mLAu@Pt NPs can induce obvious LED luminescence, suggesting that the hydrogel has good electrical conductivity. Previous studies have shown that the occurrence of MI is not only accompanied by apoptosis of myocardial cells, changes in the myocardial microenvironment but also accompanied with biochemical and mechanical-specific changes in the entire myocardium and a typical electrical conduction block. Therefore, the conductive properties of scaffold materials are very essential for the repair of MI. In recent years, combining different types of conductive nanomaterials with traditional biomaterials can significantly improve the electrical conductivity of the composite biomaterial,[24−26] endowing them with the characteristics of regulating the conductive microenvironment of MI. Significant progress has been made in the repair of MI. In this study, Au@Pt NPs were combined with natural Alg hydrogel to improve the electrical conductivity of hydrogel and effectively simulate the electrical conductivity microenvironment of natural cardiac tissue. These results laid the foundation for the subsequent promotion of electrical conduction and electrical integration in the MI region and the ultimate goal of cardiac regeneration.

According to the report, Au@Pt NPs show an excellent antioxidant property.[27] To further verify the ability of Au@Pt NPs to scavenge ROS, scavenging activity against hydroxyl radical (•OH) and 1′-diphenyl-2-picohydrazide free radical (DPPH) were detected. Au@Pt/Alg hydrogel showed higher scavenging ability of·OH and DPPH (Figure 2h.i). It further verified the scavenging efficiency of H_2O_2. Studies have shown that Au@Pt NPs can effectively catalyze H_2O_2 to produce H_2O and O_2,[28] thus realizing the antioxidant function. The results showed that Au@Pt/Alg hydrogel had significant H_2O_2 scavenging ability compared with Alg hydrogel alone (Figure 2j). The oxidation resistance of Au@Pt NPs mainly comes from the electronic structure and high catalytic performance of Pt deposited on the gold surface, which is the main reason for scavenging ROS.[17,29] This is conducive to the removal of harmful hydroxyl radicals, H_2O_2 and other ROS in the MI

https://doi.org/10.1021/acsnano.2c07436
ACS Nano 2023, 17, 2053−2066

region, so as to achieve the purpose of reshaping the MI microenvironment.

The Role of Au@Pt NPs on the CMs and Macrophage in the ROS Microenvironment. The survival and electrical integration of CMs treated with Au@Pt NPs was detected first. The primary isolated CMs were treated with Au@Pt NPs (0, 0.2, 0.5, 1, and 2 mg/mL) for 3 d. The 2 mg/mL Au@Pt NPs showed a significant inhibition of CMs activity (Figure S4). Therefore, we finally chose 1 mg/mL Au@Pt NPs for subsequent experiments. Next, the viability of CMs treated with 200 μM H_2O_2 was detected under ROS microenvironment. Addition of Au@Pt NPs improved CM survival in oxidative stress. (Figure 3a). It is speculated that Au@Pt NPs played a crucial role in reducing oxidative stress damage of CMs by scavenging ROS. We found Au@Pt NPs can effectively upregulate the expression of cx43 and c-TnT in CMs under ROS microenvironment and, at the same time, significantly inhibit the expression of apoptosis-related caspase-3 by QPCR detecting, (Figure S5). Immunofluorescence images of c-TnT and Cx43 were used to visualize (Figure 3b). Relevant results confirmed that Au@Pt NPs could protect CMs from ROS injury, enhance the expression of Cx43.

We used a multielectrode array (MEA) to detect the regional frequency of electrical pulse discharge and field potential of CMs under Au@Pt NPs. According to Figure 3c–e, after adding Au@Pt NPs, the regional field potential amplitude and its action potential frequency generated by CMs were both larger than those generated by CMs under normal culture. More interestingly, the addition of Au@Pt NPs could also improve field potential amplitude and action potential frequency of CMs under ROS microenvironment, suggesting the Au@Pt NPs can enhance the electrical pulse propagation. In this study, the electrochemical performance of CMs at the cellular level was detected by MEA which was consistent with reports that conductive nanomaterials could promote synchronous contraction and electrical propagation of CMs.[30]

Oxidative stress and inflammatory activation in early MI is the critical mechanisms of MI. When primary immune cells infiltrate an infarcted myocardium, a large number of inflammatory factors are secreted and released by macrophages. This further contributed to the exacerbation of myocardial injury.[31,32] Based on this, the anti-inflammatory effect of Au@Pt NPs *in vitro* was evaluated. First, we added Au@Pt NPs into culture medium of, and examined the expression of the M1-associated macrophages (Figure 3f). It was found that adding Au@Pt did not significantly increase the number of CD86-positive cells *in vitro*. Moreover, Au@Pt can effectively reduce the differentiation of macrophages into M1-type macrophages in the presence of H_2O_2. A series of studies have shown that Au@Pt NPs can decompose H_2O_2 into H_2O and O_2,[33] which may be the main factor for the antioxidation and inflammation reduction of Au@Pt NPs.

Further, the expression of inflammatory related genes (tumor necrosis factor α (TNF-α), C−C mode-chemokine ligand 2 (CCL-2), pro-inflammatory inducible nitric oxide synthase (iNOS)) in BMDMs was evaluated by QPCR (Figure 3g). The result showed that Au@Pt NPs could effectively reduce the H_2O_2-induced inflammatory response, and the pro-inflammatory gene expression was significantly reduced. During this process, the expression of anti-inflammatory factor (transforming growth factor β (TGF-α), Arginase1 (Arg1), and IL-10) did not change significantly (Figure S7).

Survival and Differentiation of BASCs in Au@Pt/Alg Hydrogel. The effect of Au@Pt/Alg hydrogel carrying BASCs was detected. First, alamar blue solutions were used to evaluate the effects of Au@Pt/Alg (0, 0.2, 0.5, 1, and 2 mg/mL) on the activity of BASCs cultured at 3, 7, and 14 days. The Au@Pt/Alg hydrogel (2 mg/mL) exhibited an obvious viability inhibition of BASCs (Figure 4a). The result of live/dead staining was consistent with alamar blue solutions (Figure S8). 3D imaging showed the distribution of BASCs even in Au@Pt/Alg hydrogel (Figure 4b). The activity of BASCs in Au@Pt/Alg hydrogel under H_2O_2-induced oxidative stress was further evaluated. As shown in Figure S9, the activity of BASCs in Au@Pt/Alg hydrogels was significantly increased compared with that in Alg hydrogels. It suggested that Au@Pt can effectively promote BASCs survival in hydrogel under H_2O_2-induced oxidative stress condition. In addition, we confirmed the addition of Au@Pt promoted BASCs differentiation into CMs in hydrogel by immunofluorescence staining (Figure 4c), At the same time, the differentiation of BASCs into CMs was enhanced in Au@Pt/Alg hydrogel in the ROS microenvironment (Figure 4d). This may be related to the antioxidant function of Au@Pt, which can induce BASCs differentiation into CMs in Au@Pt/Alg hydrogel by scavenging H_2O_2.

The hydroxyl radical levels of BASCs in Au@Pt/Alg hydrogel were further validated by dehydroretinol (DHE) staining. The fluorescence intensity of DHE in BASCs in Au@Pt/Alg hydrogel was decreased compared with that of Alg hydrogel when H_2O_2 existed. It is suggested that Au@Pt/Alg hydrogel can significantly reduce the level of hydroxyl radical of BASCs in Au@Pt/Alg hydrogel (Figure 4e). Relevant results have proved that Au@Pt/Alg hydrogel can improve the viability of BASCs through effective removal of ROS. At the same time, the paracrine of BASCs in Au@Pt/Alg hydrogel was evaluated by ELISA kit. More VEGF was secreted by BASCs in Au@Pt/Alg hydrogel than in Alg hydrogel under both normal and 200 μM H_2O_2 culturing, suggesting that Au@Pt/Alg hydrogel can effectively promote the paracrine level of BASCs in ROS environment (Figure 4f). The above results confirmed that Au@Pt/Alg hydrogel carrying BASCs can not only effectively promote the survival of BASCs in ROS environment but also promote the differentiation and paracrine of BASCs, providing a theoretical basis for subsequent treatment of MI with Au@Pt/Alg hydrogel.

Antioxidant, Anti-inflammatory, and Angiogenesis of Au@Pt/Alg Hydrogel Carrying BASCs in the MI Region. First, 1 and 2 mg/mL Au@Pt/Alg hydrogel were transplanted into the normal heart and subcutaneous to detect the biocompatible after 7 days, 14 days, and 1 month, respectively. H&E staining showed that there was no significant inflammatory response and no significant CD86 positive M1-type macrophages was observed by immunofluorescence staining in the heart and subcutaneous after 7 days, 14 days, and 1 month in 1 mg/mL Au@Pt/Alg hydrogel injection group. However, there was a significant infiltration of inflammatory cells and CD86 positive M1-type macrophages at 7 and 14 days in 2 mg/mL Au@Pt/Alg hydrogel injection group. While the distribution of CD86 positive macrophages decreased after 1 month in 2 mg/mL Au@Pt/Alg hydrogel injection group (Figures S10 and S11). The expression of relevant inflammatory factors was detected by QPCR, and the relevant results were consistent with the above results (Figure S12). Relevant results have proved that 1 mg/mL Au@Pt/Alg showed good biocompatibility. Further, encouraged by the *in*

https://doi.org/10.1021/acsnano.2c07436
ACS Nano 2023, 17, 2053−2066

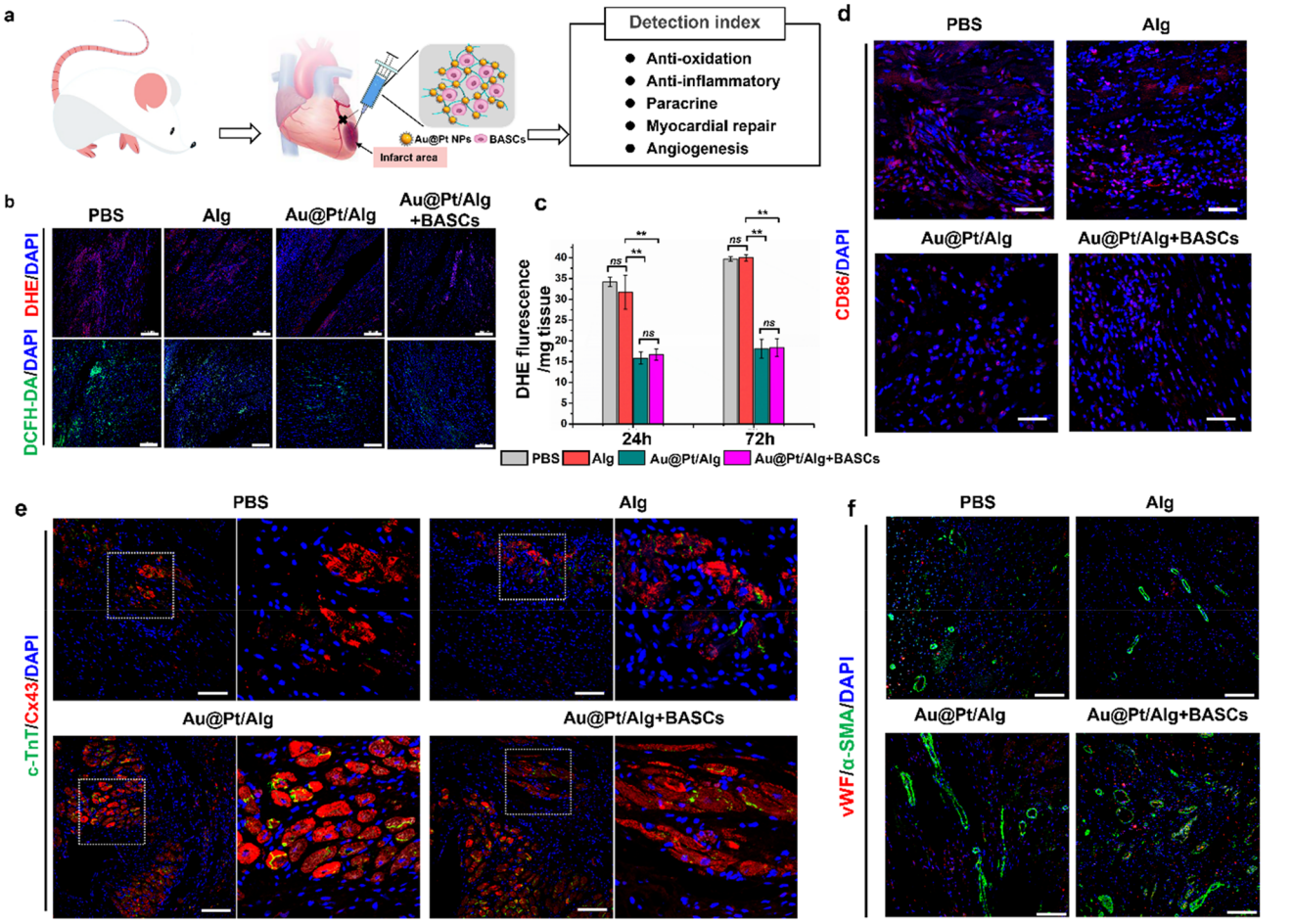

Figure 5. Effect of Au@Pt/Alg hydrogel carrying BASCs on MI *in vivo* in the different stages. (a) The detection index of the myocardial repair with Au@Pt/Alg hydrogel carrying BASCs. (b) Fluorescent images of the DHE and total intracellular ROS (DCFH-DA) of heart sections after 1 day' treatments. (c) Quantification of DHE after 1day and 3 days' treatments. (d) Immunofluorescence images of CD86 in the MI region after 1day' treatments. (e) Immunofluorescent images of c-TnT and Cx43 in the MI region after 28 days treatments. Lower panels show higher magnification images of the regions marked by white boxes in the corresponding upper panels. (f) Immunohistochemical images of vWF and α-SMA in the MI region after 28 days treatments with MI (mean ± SD, $n = 6$, *$p < 0.05$, **$p < 0.01$, Student's t test). Scale bar: 100 μm.

vitro results and biocompatibility results, we studied the antioxidant, anti-inflammatory, myocardial repair and angiogenesis at different stages. (Figure 5a). In order to verify that Au@Pt/Alg hydrogel can regulate ROS microenvironment, the levels of superoxide anion and hydroxyl radical were observed in the MI region. As shown in Figure 5b, significant DHE and DCFH-DA signals were detected inPBS group, indicating that there was a considerable accumulation of ROS in the infarct region. While the fluorescence of DHE and DCFH-DA decreased significantly after injecting Au@Pt/Alg hydrogel. The antioxidant property was verified by DHE staining kit (Figure 5c).

According to the report, necrotic CMs release alarm proteins to activate innate immune signaling pathways after MI. Anti-inflammatory mononuclear macrophages rapidly recruit and release abundant pro-inflammatory factors, resulting in an inflammatory response on days 1−3. To analyze the inflammatory response of the MI region after injecting Au@Pt/Alg hydrogel, the expression of inflammatory surface biomarkers and genes were detected by immunofluorescence staining and QPCR. CD86-positive macrophages showed a significant reduction (Figure 5d) in the Au@Pt/Alg hydrogel group and the Au@Pt/Alg carrying BASCs group compare with PBS and Alg groups. Further, a downregulation of inflammatory iNOS and TNF-α expression was verified by QPCR analysis at early MI (day 3) (Figure S13). These results confirmed that Au@Pt/Alg hydrogels have a perfect anti-inflammatory effect.

To further clarify the therapeutic effect of different injection groups *in vivo*, heart samples were collected after 28 days. The hearts inAu@Pt/Alg hydrogel injection group and Au@Pt/Alg carrying BASCs injection group showed smaller infarct size compared with the PBS injection group or Alg hydrogel injection group (Figure S14). In addition, the myocardial structure and gap junction formation were observed after 28 days' treatment in the infarct region (Figure 5e). It showed that the c-TnT and Cx43 were significantly lower after injecting PBS and Alg hydrogel, and the striatal structure of CMs was basically not observed. Nevertheless more c-TnT postive cells survived in the infarcted area after injecting Au@Pt/Alg hydrogel and Au@Pt/Alg carrying BASCs. These results indicated the survival of CMs in Au@Pt/Alg hydrogel. The high expression of Cx43 indicates remodeling of gap junctions in the Au@Pt/Alg hydrogel group, which is critical

https://doi.org/10.1021/acsnano.2c07436
ACS Nano 2023, 17, 2053−2066

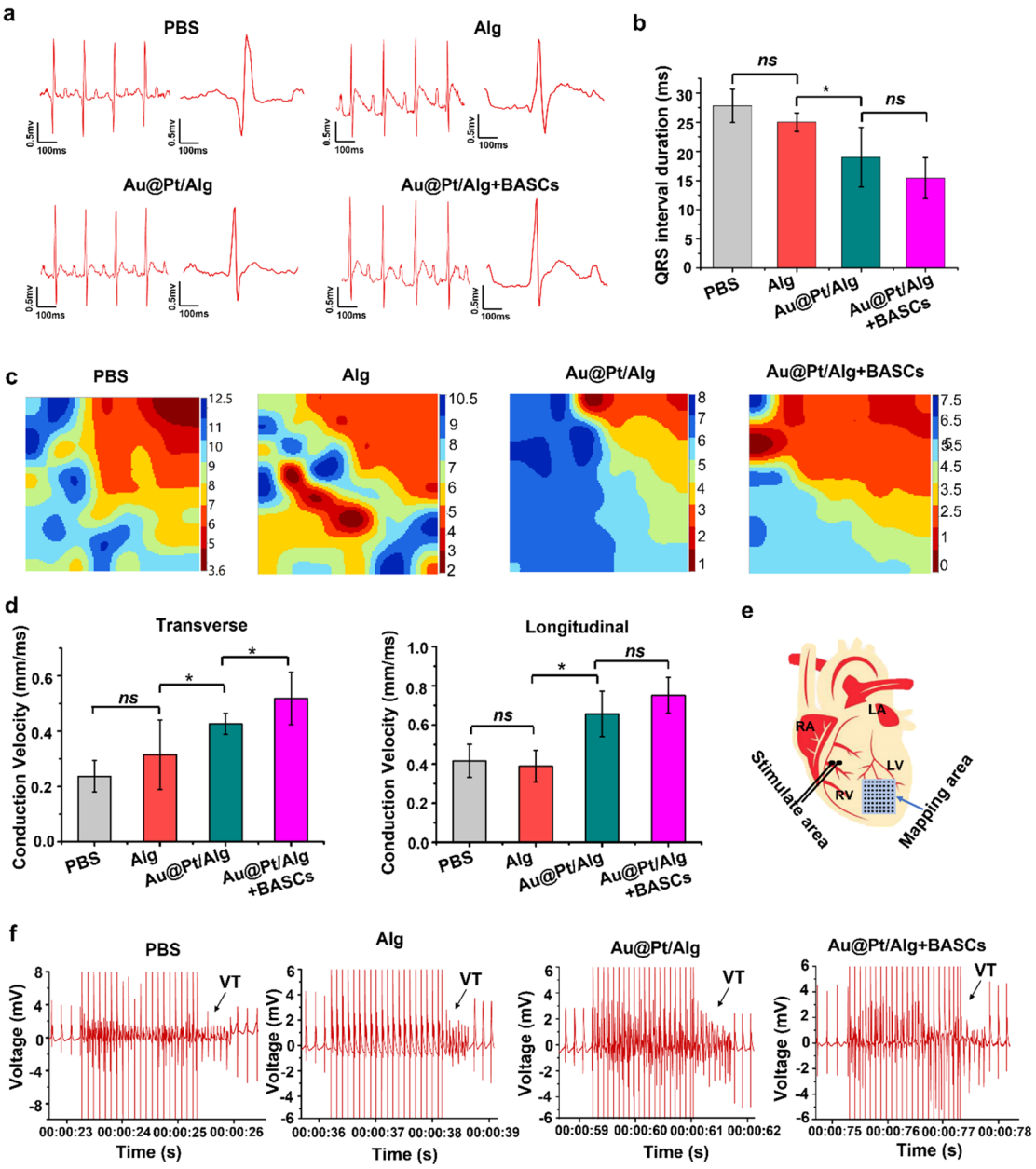

Figure 6. Effects of Au@Pt/Alg hydrogel carrying BASCs on electrical conduction reconstruction. (a) ECG recordings after 28 days' treatment and (b) QRS duration determined according to ECG. (c) Representative epicardial activation maps located on the border between the noninfarcted myocardium and infarcted myocardium after 28 days' treatment. (d) Transverse conduction velocity and longitudinal conduction velocity were calculated based on epicardial activation maps. (e) Schematic diagram of PES. (f) Electrograms of induced arrhythmias recorded after 28 days' treatment after PES (mean ± SD, $n = 6$, $^{*}p < 0.05$, $^{**}p < 0.01$, Student's t test).

for cardiac repair. Moreover, myocardial cells with horizontal striation structure in the infarct area were also clearly observed in the Au@Pt/Alg carrying BASCs group. This may be CM derived from the differentiation of transplanted BASCs in the MI region.

Angiogenesis is essential for reoxygenation and rescue CMs when MI occur.[34] Therefore, this studied focused on the effect of the Au@Pt/Alg hydrogel on vascularization in the MI region (Figure 5f). Immunofluorescence staining of α-smooth muscle actin (α-SMA) and the von Willebrand factor (vWF) were used to assess the vascular density. Compared with the PBS and Alg hydrogel group, the Au@Pt/Alg hydrogel group significantly promoted the formation of neovascularization. Meanwhile, the highest arteriolar density, especially the vWF-positive cells, was observed in the Au@Pt/Alg hydrogel-carrying BASCs group. In addition, VEGF secretion was detected by ELISA at 1 and 2 weeks after MI. The results showed that the Au@Pt/Alg hydrogel carrying the BASCs group can secrete more VEGF (Figure S15). The increasing secretion of VEGF may be because of the fact that the Au@Pt/Alg hydrogel can effectively retain and promote the activity and paracrine ability of BASCs and promote the secretion of VEGF factor and the formation of neovascularization in the MI region.

Electrical Integration of Au@Pt/Alg Hydrogel Carrying BASCs in the MI Region. Studies have shown that repairing the electrical conductivity in the MI region is very important for the recovery of heart function.[35] According to

https://doi.org/10.1021/acsnano.2c07436
ACS Nano 2023, 17, 2053−2066

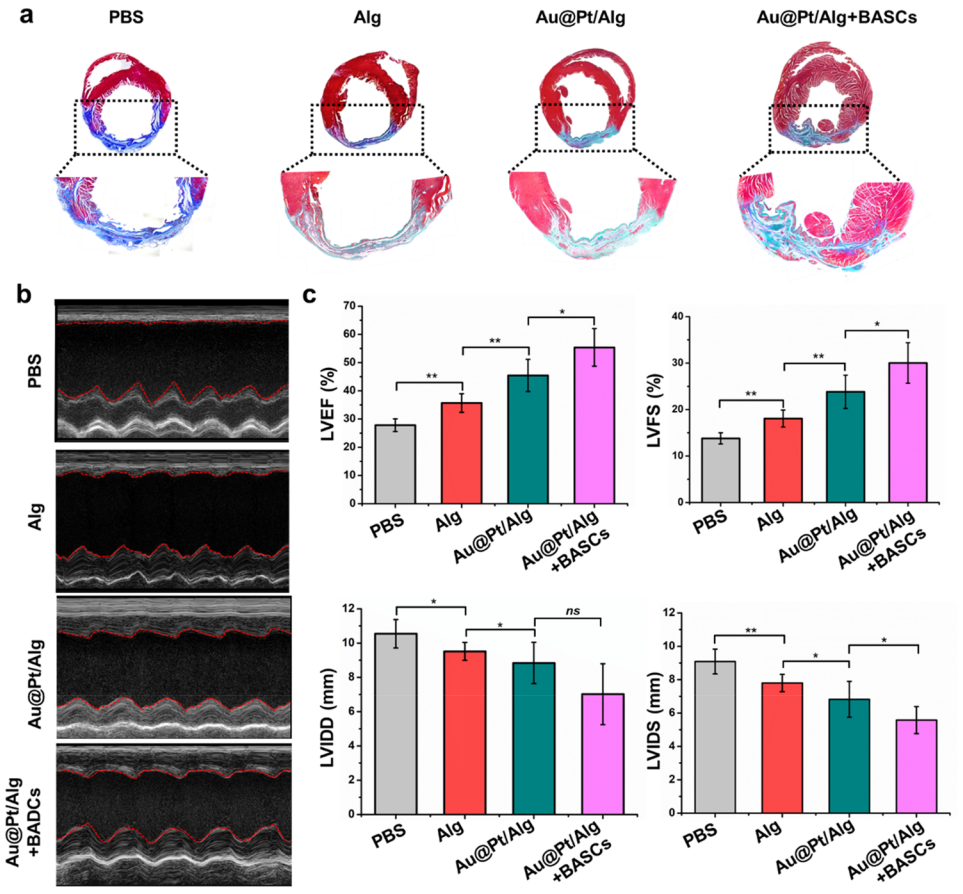

Figure 7. Effect of Au@Pt/Alg hydrogel carrying BASCs on cardiac structure of infarcted hearts and recovery of cardiac function after 28 days' treatment. (a) Masson's trichrome staining images of border zone and infarct zone of infarcted hearts after different treatments for 28 days, n = 8. (b) Echocardiographic images of MI rats in PBS, Alg hydrogel, Au@Pt/Alg hydrogel, and Au@Pt/Alg hydrogel carrying BASCs groups and (c) related LVEF, LVFS, LVIDD, and LVIDS analysis (mean ± SD, n = 8, *p < 0.05 and **p < 0.01, Student's t test).

the characteristics of electrical conductivity of myocardial cells in the MI region, a series of conductive nanomaterials in recent years has effectively promoted the research of MI repair based on injectable strategies.[36] It has been reported that conductive biomaterials can connect the normal area with the MI area, providing a timely response to electrical signals to improve the scar tissue's electrical conductivity. They can prevent arrhythmias and strengthen the synchronous contraction of the infarcted heart, improving cardiac function.[37,38] The *in vitro* experiments proved that Au@Pt had excellent electrical conductivity promoting properties of CMs. Therefore, we further verify the influence of Au@Pt/Alg carrying BASCs on conductivity characteristics and electrical integration degree in the MI region. First, QRS durations were evaluated in different treatment groups by surface ECG recordings (Figure 6a,b). Previous works have showed that "widened" QRS ofter occur in myocardial scars. We found that the duration of QRS increased significantly after MI and it did not change considerably in the Alg group. Nevertheless, the duration of QRS was significantly shortened in both the Au@Pt/Alg hydrogel group and the BASCs carrying group.

Furthermore, the electrical propagation of MI was obtained in different groups by electrical mapping and velocities of electric conduction was calculated. Using isolated Langendorff perfusion system, rat hearts in different groups were detected by epicardial activation mapping. The electrode was placed between the healthy tissue and the infarcted tissue for detection. The red part represents the excitation site first, the blue part represents the excitation site next to the red part, and the direction of excitation conduction is from red to blue. We clearly saw that the conduction direction of the normal heart is clear and orderly (Figure S16a). The electrical propagation was delayed in the PBS group and Alg group, while the Au@Pt/Alg hydrogel and Au@Pt/Alg hydrogel carrying BASCs group accelerated the excitation propagation (Figure 6c). In addition, the Au@Pt/Alg hydrogel showed higher conduction velocity regardless of whether it carried BASCs or not.

Studies have shown that weak excitatory scar tissue in MI can block the transmission of electrical signals from non-infarcted myocardium, which may lead to ventricular arrhythmias. To determine whether the injection of Au@Pt/Alg hydrogel may effectively reduce cardiac arrhythmias, we used a standard clinical PES protocol.[30,39] According to Figure S16b, normal hearts are less likely to develop arrhythmias under PES challenge. Still, regardless of whether they carry BASCs or not, infarcted hearts injected with Au@Pt/Alg hydrogels are significantly less susceptible to arrhythmias than those injected with PBS and Alg hydrogel when challenged with PES (Figure 6e–j and Figure S17). The improvement of electrical integration may be related to many mechanisms. First, Au@Pt/Alg hydrogel can improve the propagation of electrical pulses through scar tissue, which improves cardiac function by allowing living myocardium isolated by infarct scar

https://doi.org/10.1021/acsnano.2c07436
ACS Nano 2023, 17, 2053−2066

to contract simultaneously and promoting synchronous contraction with healthy myocardium. In addition, increased electrical conduction in scars may reduce the number of one-way outlet blockades of electrical signals, thereby reducing the possibility of a return circuit forming in ventricular arrhythmias.

Cardiac Function Repair of Au@Pt/Alg Hydrogel Carrying BASCs. The cardiac function repair in the MI rat model was subsequently evaluated. Notably, Masson staining showed the least fibrosis in both the infarct and boundary areas in the Au@Pt/Alg hydrogel group (Figure 7a). In particular, the left ventricular (LV) wall thickness was significantly increased in the Au@Pt/Alg hydrogel-carrying BASCs group. The Au@Pt/Alg hydrogel carrying BASCs group also showed a significant reduction in infarct size, and most fibrotic tissue returned to normal myocardium. Finally, cardiac function was assessed by echocardiography (Figure 7b). It showed classic myocardial infarction features with significantly reduced left ventricular fraction shortening (LVFS) and left ventricular ejection fraction (LVEF) shown in the PBS group. The improvements of LVEF were limited in the Alg hydrogel group, approximately 10%, which was comparable to previous reports.[40] Notably, a significant increase in LVEF and LVFS and a significant decrease in LVIDS and LVIDD were found in the Au@Pt/Alg hydrogel group and Au@Pt/Alg hydrogel carrying BASCs group, indicating that pumping function and ventricular filling was improved (Figure 7c). In this study, the Au@Pt/Alg hydrogel can effectively regulate the infarcted microenvironment, promote myocardial electrical conduction, and significantly improve cardiac function with the help of stem cells.

CONCLUSIONS

Given the electrophysiological microenvironment and the pathological microenvironment characteristics of ROS damage in the early stage of MI, this study prepared Au@Pt/Alg hydrogels with relatively simple composition, simple operation, and controllable biosafety. We found that the addition of Au@Pt NPs can not only endow Alg hydrogel with antioxdiant and anti-inflammatory functions but also introduce conductive properties. Au@Pt NPs could effectively eliminate ROS against oxidative stress damage, enhance the frequency of action potential release of cardiomyocytes, and further reduce the inflammatory factors of macrophage in ROS microenvironment *in vitro*. In addition, it plays an key role in effectively scavenging ROS and inflammatory microenvironment while accelerating electrical conduction in the MI area. Furthermore, the repair effect of MI was promoted by improving the retention and survival of implanted BASCs and angiogenesis. The related research results illustrate the advantages of Au@Pt/Alg hydrogel and its potential value as a stem cell carrier in cardiac repair.

EXPERIMENTAL SECTION

Materials. Chloroauric acid ($HAuCl_4$), chloroplatinic acid (H_2PtCl_6), and ascorbic acid (AA) were obtained from Sinopharm Group Co. Ltd. (China). Pluronic F127 ($EO_{106}PO_{70}EO_{106}$, Mw ~ 12 600 Da) was purchased from Sigma-Aldrich (USA). Dihydroethylpyridine (DHE), 2′,7′-dichlorodifluorofluorescein diacetate (DCFH-DA), 4′,6-diamidino-2-phenylindole (DAPI), hydrogen peroxide (H_2O_2) solution (30%), and ferrous sulfate heptahydrate ($FeSO_4 \cdot 7H_2O$) were purchased from Beijing Chemical Co., China. Dulbecco's Modified Eagle's Medium (DMEM), Roswell Park Memorial Institute (RPMI) 1640 medium, fetal bovine serum (FBS), penicillin−streptomycin, and trypsin were purchased from Gibco, NY, USA. The antibodies of cardiac troponin T (c-TnT), gap connexin 43 (CX43), CD86, von Willebrand Factor (vWF), α-smooth muscle actin (α-SMA), and the enzyme-linked immunosorbent assay (ELISA) test kits of VEGF were purchased from Abcam (Cambridge, U.K.). Tissue ROS detection kit (DHE) was purchased from Biorab Biotech.

Au@Pt/Alg Hydrogel Preparation. The preparation of Au@Pt/Alg hydrogel required two steps. In a typical synthesis of Au@Pt nanoparticles according to a reported protocol (Pt/Au molar ratio = 1.0),[22] 3 mL of H_2PtCl_6 solution (20 mM) and 3 mL of $HAuCl_4$ solution (20 mM) were mixed with Pluronic F127 (60 mg). In the following step,, 6 mL of AA solution (0.1 M) was added, and the mixture was sonicated for 15 min. The mixture was then aged for another 24 h. After centrifugation at 12500 rpm for 10 min, the products were washed three times with 50% ethanol and dispersed in water for further use. Further preparation of the antioxidant hydrogel, Au@Pt was added into the alginate solution (3 wt %), and the final concentrations of Au@Pt were 0, 0.2, 0.5, 1, and 2 mg/mL. Next add calcium gluconate solution (3 wt %) into the calcium Au@Pt/Alg solution as in a volume ratio of 1:3 and continue to stir. After stirring, different Au@Pt/Alg hydrogels were incubated at 37 °C for 5−10 min.

Characterization of Au@Pt/Alg Hydrogel. The gelation of different hydrogels were investigated through the method of test tube inversion and their rheological behaviors were studied using a controlled stress rheometer (HR 1, TA Instrument, USA) with 10 mm flat plates. The pore size and surface morphology of the Au@Pt/Alg hydrogel were detected by scanning electron microscopy (Zeiss Supra55).

The electroactivity of the hydrogels including the conductivity and cyclic voltammetry (CV) properties were measured using a four-probe method (RTS-8 four-probe resistivity meter, China) and an electrochemical workstation (CHI660E, Shanghai Chenhua, China), respectively. The conductivity of 1 mg/mL Au@Pt/Alg hydrogel was measured by LED circuit experiment. The CV curves of Au@Pt/Alg hydrogel (0, 0.2, 0.5, 1, and 2 mg/mL) between −0.5 and +1 V potentials were collected at a scanning rate of 50 mV s^{-1} in phosphate buffer saline (PBS, 0.1 M, pH = 7.4).

The antioxidant properties of Au@Pt/Alg hydrogel were detected by evaluating their hydroxyl radicals and 1′-diphenyl-2-picrylhydrazyl (DPPH) radicals' scavenging capability. Briefly, 300 mm^3 Au@Pt/Alg hydrogel was added into a mixture solution which was prepared by mixing 2 mM $FeSO_4$ solution and 360 μg/mL Safranin O solution (volume ratio: 6:5) and the deionized water was as the blank group. Then, 800 μL of H_2O_2 (6 wt %) or deionized water was added into the solution and the mixed solution was incubated at 55 °C for 60 min. The absorbance of the reaction mixtures at 492 nm were measured by a enzyme-labeled instrument (Molecular Devices). To evaluate the effect of scavenging DPPH free radicals, 300 mm^3 hydrogel with deionized water as a control can be soaked in 800 μL of DPPH solution in the dark for 1 h. The OD value at 517 nm was then detected using a microplate reader. A typical colorimetric detection for Cys was conducted to detected scavenging H_2O_2 ability. First, 100 μL of a different concentration of Au@Pt/Alg hydrogel was added into 500 μL of a NaAc−HAc solution (0.2 M), and then 1 mL of Cys

https://doi.org/10.1021/acsnano.2c07436
ACS Nano 2023, 17, 2053−2066

solution with different concentrations of Cys was added. Second, all the solutions were incubated at 37 °C for 15 min. Finally, the above solution was added with 200 μL of H_2O_2 (0.1 M) and 200 μL of TMB (2.5 mM) successively. After a 10-min reaction at 37 °C, the 652 nm absorbance signals of the above solutions were measured using UV−vis spectroscopy.

Assessment of Cardiomyocytes Activity and Electrical Conductivity under ROS Conditions by Au@Pt Treatment. CMs was treated by different concentrations of Au@Pt NPs (0, 0.2, 0.5, 1, and 2 mg/mL) for 3 days. The CMs cultured medium was replaced with 10% Alamar Blue solution. The absorbance of the supernatant was detected after another 4 h culture. Next, 200 μM H_2O_2 and 1 mg/mL Au@Pt NPs was introduced to the culture medium for 24 h. The Alamar Blue assay was used to assess the CMs viability in the ROS microenvironment. Further, relative expressions of cardiac troponin T (c-TnT), apoptosis-related gene caspase-3, and gap connexin 43 (CX43) were evaluated using qRT-PCR and immunofluorescence staining assay.

The CMs were seeded on MEA electrode (EGMA064200700A) and cultured for 48 h. Then the CMs were given different treatment (normal culture, 1 mg/mL Au@Pt NPs treatment, 200 μM H_2O_2 treatment, 200 μM H_2O_2, and 1 mg/mL Au@Pt NPs coordinate treatment) for 24 h. The electrical activity of CMs were investigated by the electric signal recorder (EMS64-USB-1003). MEA electrodes were inoculated with CMs at 37 °C temperature to maintain the activity of the CMs. The frequency of electric pulse and the amplitude of field potential were calculated according to the recorded frequency spectrum.

Evaluation of Anti-inflammatory Activity In Vitro. One mg/mL of Au@Pt NPs was added to the culture medium of BMDMs under 200 μM H_2O_2. Relative expressions of pro-inflammatory (CD86, iNOS, and TNF-α) genes and proteins were evaluated using qRT-PCR immunofluorescence staining assay.

Viability and Antioxidant Ability of BASCs in Au@Pt/Alg Hydrogel. The BADCs were seeded in different concentrations of Au@Pt/Alg hydrogel (0, 0.2, 0.5, 1, and 2 mg/mL) for 3 and 7 days culturing. The samples were treated by live/dead staining for 30 min in the dark and live and dead cells were detected by confocal laser scanning microscope (CLSM, Nikon Ti A1) to evaluate the cytocompatibility of BASCs in Au@Pt/Alg hydrogel. At the same time, the samples' cultured medium was replaced with medium containing 10% alamar blue solutions. Additional 4 h culturing was performed before the absorbance was measured by a microplate reader (Molecular Devices, at 570).

The intracellular superoxide anions level was evaluated by a dihydroethidium (DHE) staining kit. Briefly, BASCs in Au@Pt/Alg hydrogel were cultured for 24 h in normal or 200 μM H_2O_2-induced ROS microenvironment. The samples were incubated with DHE for 15−25 min. Cell nucleuses were stained by 4′,6-diamidino-2-phenylindole (DAPI) after washing with PBS and were observed under CLSM.

Establish MI Model and BADSCs-Laden Hydrogel Injection. Male Sprague−Dawley rats (250 ± 20 g) were anesthetized by intraperitoneal injection of 2% sodium pentobarbital. After a left thoracotomy was performed, the proximal left anterior descending artery (LAD) underwent ligation surgery using 6−0 polypropylene suture. Next, different materials were injected in the MI area and MI functional area. The MI rats were randomly divided into four groups: (1) PBS (100 μL; n = 8); (2) Alg hydrogel (100 μL; n = 8); (3) Au@Pt/Alg hydrogel (100 μL; n = 8); (4) Au@Pt/Alg hydrogel + BASCs (100 μL; BASCs: 5×10^6, n = 8). These mixed solutions were rapidly injected in the infarction and border area with a 28-gauge needle. Then, the thoracic cavities were closed in multiple layers. All animal experiments were performed in accordance with the National Institutes of Health (NIH Publications) and approved by the Institutional Animal Care and Use Committee (IACUC).

In Vivo Measurement of Intracellular ROS in Rat Infarct Model. To measure the intracellular ROS in vivo after different treatment, DHE (Sigma) and DCFH-DA (Sigma) stainings were performed. The heart sections from MI areas were collected at 24 h, and then the samples in different groups were incubated with DHE (5 mM) or DCFH-DA (10 μM) solution for 10−20 min. After using PBS to wash, the heart sections were counterstained by DAPI (Sigma) and were examined under CLSM. In addition, DHE content in heart tissue was measured by ROS detection kit (DHE). Briefly, fresh heart tissue was obtained at day 1 and day 3. Then, 50 mg of tissue from each group was disposed by 1 mL of homogenization buffer, and the heart tissue supernatant was then collected and detected. The supernatant and DHE probe were added according to the protocols and the mixture was incubated at 37 °C for 0.5 h. Finally, the fluorescence intensity was determined via a microplate reader (excitation wavelength 535 nm).

Immunohistochemistry for Evaluation Inflammation, Myocardial Structure, and Angiogenesis. To evaluate the anti-inflammatory, myocardial structure, and angiogenesis after different treatment. The heart sections from MI areas were fixed in 4 wt % paraformaldehyde at 24 h for inflammation detection, and myocardial structure and angiogenesis was detected at 4 weeks after hydrogel injection. Briefly, the fixed hearts were dehydrated by gradient ethanol dehydration, made transparent by xylene, embedded in paraffin, and sectioned to obtain the 4 μm heart sections. For immunofluorescence staining, heart sections were permeabilized in 0.1% Triton X-100 for 30 min, and then blocked with bovine serum for 30 min. Primary antibodies were used to incubated the heart sections overnight at 4 °C for detection of M1 macrophage (rabbit anti-CD86 Abcam). Subsequently, the sections were washed with PBS and then incubated with secondary antibodies (Cy3-labeled, goat antirabbit IgG, BosterBio) for 90 min. Cell nuclei were stained with DAPI. At the same time, for myocardial structure evaluation, the heart sections were incubated with c-TnT and Cx43 antibodies. To evaluate the new vessels forming, vWF and anti-α-smooth muscle actin antibodies were used to incubate heart sections. Immunofluorescence staining of all heart sections was then visualized using CLSM.

Assessment of Electrical Integration. The propagation of electrical signals in scar tissue was evaluated with an electrical stimulation generator (DS8000) and an ECG recorder (PL3516). The scar tissue was collected after the rat was sacrificed (3 mm healthy tissue was preserved at both ends of the scar tissue). The end of the tissue was connected to the electrical stimulator and ECG recorder, respectively. The settings of the electrical stimulator were as follows: 10 mV and 1 Hz. After 4 weeks, a 5 min recording of ECG was collected with three surface leads. These recordings were analyzed with Lab Chart to obtain QRS durations. Arrhythmia induction rates were determined according to a standard clinical

https://doi.org/10.1021/acsnano.2c07436
ACS Nano 2023, 17, 2053−2066

electrical stimulation (PES) protocol.[30] The data were quantified as induction rates according to an reported scoring system.

Epicardial activation mapping between healthy and infarct myocardium was examined using the electrophysiological mapping system with 64 channels (MappingLab). After the heart was isolated and underwent Langendorff perfusion, the 64-channel electrode (8 × 8 grids, 0.45 mm spacing) were placed at the border area. Electrical stimulation (2 mV, 4 Hz) was applied to the epicardium under the left ear of the heart. According to the report, the activation time is determined by the point of maximum negative slope. The first stable waveform was selected for the activation time analysis, and all isochrones were produced as the areas activated per 2 ms.

Echocardiography for Evaluation Cardiac Functions. The function of the left ventricular (LV) muscle was investigated by echocardiograms for different group of MI at 4 weeks after surgery. We anesthetized MI model rats and performed echocardiograms on a 13 MHz linear ultrasonic transducer (15L8; Acuson Corporation, Mountain View). LVEF, LVFS, LVIDS, and LVIDD were analyzed by experienced operating technicians.

Statistical Analysis. All data expressed as average ± SD, statistical analyses were performed with Origin Pro 8.5 software. Differences with $*P < 0.05$ or $**P < 0.01$ were considered significant. The sample sizes (n) indicate the number of either biological replicates or animals. The date from three times ($n \geq 3$) for each sample in vitro, and the number of animals is 6 or greater than per group.

ASSOCIATED CONTENT

Supporting Information

The Supporting Information is available free of charge at https://pubs.acs.org/doi/10.1021/acsnano.2c07436.

Supplementary notes S1−S5, isolation and culture of cell, CMs differentiation and paracrine of BASCs, biocompatible detection in vivo, histological analysis, and real-time PCR analysis; Table S1, sequence of primers; Figure S1−S16, particle size distributions, rheological properties, TEM image, viability of CMs, gene expression of of c-TnT, cx43, and caspase-3, flow cytometry of BASCs, expression of inflammatory genes, cytocompatibility of BASC, viability of BASCs; biocompatiblity in the heart, biocompatiblity in the subcutaneous, inflammatory factors expression after transplantation, expression of CD86, iNOS, and TNF-α, photographs of hearts, the paracrine level, and electrical mapping and electrograms (PDF)

AUTHOR INFORMATION

Corresponding Authors

Jin Zhou − *Beijing Institute of Basic Medical Sciences, Beijing 100850, China*; orcid.org/0000-0003-3128-407X; Email: sisun819@outlook.com

Changyong Wang − *Beijing Institute of Basic Medical Sciences, Beijing 100850, China*; Email: wcy2000_zm@163.com

Fu-Jian Xu − *Key Lab of Biomedical Materials of Natural Macromolecules (Beijing University of Chemical Technology, Ministry of Education), Beijing 100029, China; Beijing Laboratory of Biomedical Materials, Beijing University of Chemical Technology, Beijing 100029, China; Beijing Advanced Innovation Center for Soft Matter Science and Engineering and College of Materials Science and Engineering, Beijing University of Chemical Technology, Beijing 100029, China*; orcid.org/0000-0002-1838-8811; Email: xufj@mail.buct.edu.cn

Authors

Wei Liu − *Beijing Institute of Basic Medical Sciences, Beijing 100850, China*; orcid.org/0000-0002-3536-3915

Nana Zhao − *Key Lab of Biomedical Materials of Natural Macromolecules (Beijing University of Chemical Technology, Ministry of Education), Beijing 100029, China; Beijing Laboratory of Biomedical Materials, Beijing University of Chemical Technology, Beijing 100029, China; Beijing Advanced Innovation Center for Soft Matter Science and Engineering and College of Materials Science and Engineering, Beijing University of Chemical Technology, Beijing 100029, China*; orcid.org/0000-0001-8610-3411

Qi Yin − *Beijing Institute of Basic Medical Sciences, Beijing 100850, China*

Xiaoyi Zhao − *Key Lab of Biomedical Materials of Natural Macromolecules (Beijing University of Chemical Technology, Ministry of Education), Beijing 100029, China; Beijing Laboratory of Biomedical Materials, Beijing University of Chemical Technology, Beijing 100029, China; Beijing Advanced Innovation Center for Soft Matter Science and Engineering and College of Materials Science and Engineering, Beijing University of Chemical Technology, Beijing 100029, China*

Kangli Guo − *Key Lab of Biomedical Materials of Natural Macromolecules (Beijing University of Chemical Technology, Ministry of Education), Beijing 100029, China; Beijing Laboratory of Biomedical Materials, Beijing University of Chemical Technology, Beijing 100029, China; Beijing Advanced Innovation Center for Soft Matter Science and Engineering and College of Materials Science and Engineering, Beijing University of Chemical Technology, Beijing 100029, China*

Yifan Xian − *Key Lab of Biomedical Materials of Natural Macromolecules (Beijing University of Chemical Technology, Ministry of Education), Beijing 100029, China; Beijing Advanced Innovation Center for Soft Matter Science and Engineering and College of Materials Science and Engineering, Beijing University of Chemical Technology, Beijing 100029, China*

Siwei Li − *Beijing Institute of Basic Medical Sciences, Beijing 100850, China*

Chunlan Wang − *Beijing Institute of Basic Medical Sciences, Beijing 100850, China*

Miaomiao Zhu − *Beijing Institute of Basic Medical Sciences, Beijing 100850, China*

Yurong Du − *Beijing Institute of Basic Medical Sciences, Beijing 100850, China*

Complete contact information is available at: https://pubs.acs.org/10.1021/acsnano.2c07436

Author Contributions

⊥W.L. and N.Z. contributed equally to this work.

Notes

The authors declare no competing financial interest.

https://doi.org/10.1021/acsnano.2c07436
ACS Nano 2023, 17, 2053−2066

ACKNOWLEDGMENTS

This work was supported by the National Key Research and Development Program of China (Grant Nos. 2017YFA0106100), the National Natural Science Foundation of China (Grant Nos. 31830030, 51922022), and the Joint Fund Project of the National Natural Science Foundation of China (Grant Nos. U21A203940).

REFERENCES

(1) Lu, L.; Liu, M.; Sun, R.; Zheng, Y.; Zhang, P. Myocardial Infarction: Symptoms and Treatments. *Cell. Biochem. Biophys.* **2015**, *72*, 865−867.

(2) Majid, Q. A.; Fricker, A. T. R.; Gregory, D. A.; Davidenko, N.; Hernandez Cruz, O.; Jabbour, R. J.; Owen, T. J.; Basnett, P.; Lukasiewicz, B.; Stevens, M.; Best, S.; Cameron, R.; Sinha, S.; Harding, S. E.; Roy, I. Natural Biomaterials for Cardiac Tissue Engineering: A Highly Biocompatible Solution. *Front. Cardiovasc. Med.* **2020**, *7*, 554597.

(3) Walker, B. W.; Lara, R. P.; Yu, C. H.; Sani, E. S.; Kimball, W.; Joyce, S.; Annabi, N. Engineering a naturally-derived adhesive and conductive cardiopatch. *Biomaterials* **2019**, *207*, 89−101.

(4) Shadrin, I. Y.; Allen, B. W.; Qian, Y.; Jackman, C. P.; Carlson, A. L.; Juhas, M. E.; Bursac, N. Cardiopatch platform enables maturation and scale-up of human pluripotent stem cell-derived engineered heart tissues. *Nat. Commun.* **2017**, *8*, 1825.

(5) Yoshizaki, Y.; Ii, M.; Takai, H.; Mayumi, N.; Fujiwara, S.; Kuzuya, A.; Ohya, Y. Cellular therapy for myocardial ischemia using a temperature-responsive biodegradable injectable polymer system with adipose-derived stem cells. *Sci. Technol. Adv. Mater.* **2021**, *22*, 627−642.

(6) Hao, T.; Li, J.; Yao, F.; Dong, D.; Wang, Y.; Yang, B.; Wang, C. Injectable Fullerenol/Alginate Hydrogel for Suppression of Oxidative Stress Damage in Brown Adipose-Derived Stem Cells and Cardiac Repair. *ACS Nano* **2017**, *11*, 5474−5488.

(7) Shilo, M.; Oved, H.; Wertheim, L.; Gal, I.; Noor, N.; Green, O.; Baruch, E. S.; Shabat, D.; Shapira, A.; Dvir, T. Injectable Nanocomposite Implants Reduce ROS Accumulation and Improve Heart Function after Infarction. *Adv. Sci.* **2021**, *8*, 2102919.

(8) Xing, M.; Jiang, Y.; Bi, W.; Gao, L.; Zhou, Y. L.; Rao, S. L.; Ma, L. L.; Zhang, Z. W.; Yang, H. T.; Chang, J. Strontium ions protect hearts against myocardial ischemia/reperfusion injury. *Sci. Adv.* **2021**, *7*, No. eabe0726.

(9) Zhang, Y.; Cai, Z.; Shen, Y.; Lu, Q.; Gao, W.; Zhong, X.; Yao, K.; Yuan, J.; Liu, H. Hydrogel-load exosomes derived from dendritic cells improve cardiac function via Treg cells and the polarization of macrophages following myocardial infarction. *J. Nanobiotechnology.* **2021**, *19*, 271.

(10) Qian, B.; Yang, Q.; Wang, M.; Huang, S.; Jiang, C.; Shi, H.; Long, Q.; Zhou, M.; Zhao, Q.; Ye, X. Encapsulation of lyophilized platelet-rich fibrin in alginate-hyaluronic acid hydrogel as a novel vascularized substitution for myocardial infarction. *Bioact. Mater.* **2022**, *7*, 401−411.

(11) Zhou, J.; Liu, W.; Zhao, X.; Xian, Y.; Wu, W.; Zhang, X.; Zhao, N.; Xu, F. J.; Wang, C. Natural Melanin/Alginate Hydrogels Achieve Cardiac Repair through ROS Scavenging and Macrophage Polarization. *Adv. Sci.* **2021**, *8*, No. 2100505.

(12) Li, H.; Yu, B.; Yang, P.; Zhan, J.; Fan, X.; Chen, P.; Liao, X.; Ou, C.; Cai, Y.; Chen, M. Injectable AuNP-HA matrix with localized stiffness enhances the formation of gap junction in engrafted human induced pluripotent stem cell-derived cardiomyocytes and promotes cardiac repair. *Biomaterials* **2021**, *279*, 121231.

(13) Zhou, J.; Chen, J.; Sun, H.; Qiu, X.; Mou, Y.; Liu, Z.; Zhao, Y.; Li, X.; Han, Y.; Duan, C.; Tang, R.; Wang, C.; Zhong, W.; Liu, J.; Luo, Y.; Xing, M.; Wang, C. Engineering the heart: evaluation of conductive nanomaterials for improving implant integration and cardiac function. *Sci. Rep.* **2014**, *4*, 3733.

(14) Zhang, C.; Hsieh, M. H.; Wu, S. Y.; Li, S. H.; Wu, J.; Liu, S. M.; Wei, H. J.; Weisel, R. D.; Sung, H. W.; Li, R. K. A self-doping conductive polymer hydrogel that can restore electrical impulse propagation at myocardial infarct to prevent cardiac arrhythmia and preserve ventricular function. *Biomaterials* **2020**, *231*, 119672.

(15) Zhang, W.; Liu, J.; Li, X.; Zheng, Y.; Chen, L.; Wang, D.; Foda, M. F.; Ma, Z.; Zhao, Y.; Han, H. Precise Chemodynamic Therapy of Cancer by Trifunctional Bacterium-Based Nanozymes. *ACS Nano* **2021**, *15*, 19321−19333.

(16) Wen, T.; Yang, A.; Wang, T.; Jia, M.; Lai, X.; Meng, J.; Liu, J.; Han, B.; Xu, H. Ultra-small platinum nanoparticles on gold nanorods induced intracellular ROS fluctuation to drive megakaryocytic differentiation of leukemia cells. *Biomater. Sci.* **2020**, *8*, 6204−6211.

(17) Fan, W. T.; Qin, Y.; Hu, X. B.; Yan, J.; Wu, W. T.; Liu, Y. L.; Huang, W. H. Stretchable Electrode Based on Au@Pt Nanotube Networks for Real-Time Monitoring of ROS Signaling in Endothelial Mechanotransduction. *Anal. Chem.* **2020**, *92*, 15639−15646.

(18) Li, Y.; Shi, X.; Tian, L.; Sun, H.; Wu, Y.; Li, X.; Li, J.; Wei, Y.; Han, X.; Zhang, J.; Jia, X.; Bai, R.; Jing, L.; Ding, P.; Liu, H.; Han, D. AuNP-Collagen Matrix with Localized Stiffness for Cardiac-Tissue Engineering: Enhancing the Assembly of Intercalated Discs by β1-Integrin-Mediated Signaling. *Adv. Mater.* **2016**, *28*, 10230−10235.

(19) Bian, T.; Zhang, H.; Jiang, Y.; Jin, C.; Wu, J.; Yang, H.; Yang, D. Epitaxial Growth of Twinned Au-Pt Core-Shell Star-Shaped Decahedra as Highly Durable Electrocatalysts. *Nano Lett.* **2015**, *15*, 7808−7815.

(20) He, W.; Liu, Y.; Yuan, J.; Yin, J. J.; Wu, X.; Hu, X.; Zhang, K.; Liu, J.; Chen, C.; Ji, Y.; Guo, Y. Au@Pt nanostructures as oxidase and peroxidase mimetics for use in immunoassays. *Biomaterials* **2011**, *32*, 1139−1147.

(21) Sharma, C.; Ansari, S.; Ansari, M. S.; Satsangee, S. P. Phyto-mediated synthesis of Pt and Au/Pt bimetallic nanoparticles using Syzygium aromaticum bud-extract: Study of their catalytic, anti-bacterial, and antioxidant activities. *J. Ind. Eng. Chem.* **2022**, *111*, 499−508.

(22) Ataee-Esfahani, H.; Wang, L.; Nemoto, Y.; Yamauchi, Y. Synthesis of Bimetallic Au@Pt Nanoparticles with Au Core and Nanostructured Pt Shell toward Highly Active Electrocatalysts. *Chem. Mater.* **2010**, *22*, 6310−6318.

(23) Bao, R.; Tan, B.; Liang, S.; Zhang, N.; Wang, W.; Liu, W. A π-π conjugation-containing soft and conductive injectable polymer hydrogel highly efficiently rebuilds cardiac function after myocardial infarction. *Biomaterials* **2017**, *122*, 63−71.

(24) Bai, R.; Liu, J.; Zhang, J.; Shi, J.; Jin, Z.; Li, Y.; Ding, X.; Zhu, X.; Yuan, C.; Xiu, B.; Liu, H.; Yuan, Z.; Liu, Z. Conductive single-wall carbon nanotubes/extracellular matrix hybrid hydrogels promote the lineage-specific development of seeding cells for tissue repair through reconstructing an integrin-dependent niche. *J. Nanobiotechnology.* **2021**, *19*, 252.

(25) Shevach, M.; Fleischer, S.; Shapira, A.; Dvir, T. Gold nanoparticle-decellularized matrix hybrids for cardiac tissue engineering. *Nano Lett.* **2014**, *14*, 5792−5796.

(26) Hosoyama, K.; Ahumada, M.; McTiernan, C. D.; Davis, D. R.; Variola, F.; Ruel, M.; Liang, W.; Suuronen, E. J.; Alarcon, E. I. Nanoengineered Electroconductive Collagen-Based Cardiac Patch for Infarcted Myocardium Repair. *ACS Appl. Mater. Interfaces.* **2018**, *10*, 44668−44677.

(27) Liang, H.; Wu, Y.; Ou, X. Y.; Li, J. Y.; Li, J. Au@Pt nanoparticles as catalase mimics to attenuate tumor hypoxia and enhance immune cell-mediated cytotoxicity. *Nanotechnology* **2017**, *28*, 465702.

(28) Yang, S.; Han, G.; Chen, Q.; Yu, L.; Wang, P.; Zhang, Q.; Dong, J.; Zhang, W.; Huang, J. Au-Pt Nanoparticle Formulation as a Radiosensitizer for Radiotherapy with Dual Effects. *Int. J. Nanomedicine.* **2021**, *16*, 239−248.

(29) Song, Y.; Shi, Q.; Zhu, C.; Luo, Y.; Lu, Q.; Li, H.; Ye, R.; Du, D.; Lin, Y. Mitochondrial-targeted multifunctional mesoporous Au@Pt nanoparticles for dual-mode photodynamic and photothermal therapy of cancers. *Nanoscale* **2017**, *9*, 15813−15824.

(30) Chen, S.; Hsieh, M. H.; Li, S. H.; Wu, J.; Weisel, R. D.; Chang, Y.; Sung, H. W.; Li, R. K. A conductive cell-delivery construct as a

bioengineered patch that can improve electrical propagation and synchronize cardiomyocyte contraction for heart repair. *J. Controlled Release* **2020**, *320*, 73−82.
(31) Cadenas, S. ROS and redox signaling in myocardial ischemia-reperfusion injury and cardioprotection. *Free. Radic. Biol. Med.* **2018**, *117*, 76−89.
(32) Zhao, T.; Wu, W.; Sui, L.; Huang, Q.; Nan, Y.; Liu, J.; Ai, K. Reactive oxygen species-based nanomaterials for the treatment of myocardial ischemia reperfusion injuries. *Bioact. Mater.* **2022**, *7*, 47−72.
(33) Nguyen, H. V.; Kim, K. Y.; Nam, H.; Lee, S. Y.; Yu, T.; Seo, T. S. Centrifugal microfluidic device for the high-throughput synthesis of Pd@AuPt core-shell nanoparticles to evaluate the performance of hydrogen peroxide generation. *Lab Chip.* **2020**, *20*, 3293−3301.
(34) Vong, L. B.; Bui, T. Q.; Tomita, T.; Sakamoto, H.; Hiramatsu, Y.; Nagasaki, Y. Novel angiogenesis therapeutics by redox injectable hydrogel - Regulation of local nitric oxide generation for effective cardiovascular therapy. *Biomaterials* **2018**, *167*, 143−152.
(35) Song, X.; Wang, X.; Zhang, J.; Shen, S.; Yin, W.; Ye, G.; Wang, L.; Hou, H.; Qiu, X. A tunable self-healing ionic hydrogel with microscopic homogeneous conductivity as a cardiac patch for myocardial infarction repair. *Biomaterials* **2021**, *273*, 120811.
(36) Wang, L.; Liu, Y.; Ye, G.; He, Y.; Li, B.; Guan, Y.; Gong, B.; Mequanint, K.; Xing, M. M. Q.; Qiu, X. Injectable and conductive cardiac patches repair infarcted myocardium in rats and minipigs. *Nat. Biomed. Eng.* **2021**, *5*, 1157−1173.
(37) He, Y.; Ye, G.; Song, C.; Li, C.; Xiong, W.; Yu, L.; Qiu, X.; Wang, L. Mussel-inspired conductive nanofibrous membranes repair myocardial infarction by enhancing cardiac function and revascularization. *Theranostics* **2018**, *8*, 5159−5177.
(38) Song, C.; Zhang, X.; Wang, L.; Wen, F.; Xu, K.; Xiong, W.; Li, C.; Li, B.; Wang, Q.; Xing, M. M. Q.; Qiu, X. An Injectable Conductive Three-Dimensional Elastic Network by Tangled Surgical-Suture Spring for Heart Repair. *ACS Nano* **2019**, *13*, 14122−14137.
(39) Nguyen, T.; El Salibi, E.; Rouleau, J. L. Postinfarction survival and inducibility of ventricular arrhythmias in the spontaneously hypertensive rat: effects of ramipril and hydralazine. *Circulation* **1998**, *98*, 2074−2080.
(40) Wu, Y.; Chang, T.; Chen, W.; Wang, X.; Li, J.; Chen, Y.; Yu, Y.; Shen, Z.; Yu, Q.; Zhang, Y. Release of VEGF and BMP9 from injectable alginate based composite hydrogel for treatment of myocardial infarction. *Bioact. Mater.* **2021**, *6*, 520−528.

https://doi.org/10.1021/acsnano.2c07436
ACS Nano 2023, 17, 2053−2066